J. COMBIN. MATH. COMBIN. COMPUT. 127a (2025) 4465--4488

Journal of Combinatorial Mathematics and Combinatorial Computing
www.combinatorialpress.com/jcmcc

Combinatorial Press

Computational study of adaptive current interruption protection strategy based on multi-intelligent body system in AC-DC hybrid power grid

Wei Xu[1], Yu Sui[1,✉], Yabin Chen[1], Huazhen Cao[1]

[1] Power Grid Planning Research Center of Guangdong Power Grid Co., Ltd., Guangzhou, Guangdong, 510220, China

ABSTRACT

Aiming at the shortcomings of traditional relay protection, an adaptive multi-area protection coordination model is studied and designed. Firstly, combining different control strategies such as master-slave control and sag control, a method of AC/DC distribution network trend calculation and network loss analysis based on the alternating iteration method is proposed and realized to ensure that the adaptive relay protection can act correctly. The proposed method is analyzed for AC/DC hybrid distribution network trend calculation, and the alternating iteration solution method is used for trend analysis and calculation, and the effectiveness of the proposed method is verified by two examples of AC/DC hybrid distribution networks. Then the adaptive Agent with reinforcement learning is introduced, and its constructed multi-agent system has more system adaptive capability. The adaptive current interruption protection is compared with the traditional current interruption protection, and its protection principle and protection scope are analyzed, on the basis of which an adaptive coordinated protection method based on MAS grid is proposed to realize the MAS adaptive current interruption protection, and its simulation is verified. The experimental results show that the method of this paper can significantly improve the flexibility, effectiveness and stability of AC and DC distribution network operation.

Keywords: Hybrid AC-DC distribution network, adaptive protection, multi-agent system, current calculation, control strategy

1. Introduction

The energy crisis is one of the biggest problems faced by mankind in the 21st century, coupled with the rapid development of society, which makes the environmental pollution problem increasingly serious. Under the double pressure of energy crisis as well as environmental pollution, people begin

✉ Corresponding author.
E-mail address: SuiYu202412@126.com (Y. Sui).
Received 12 January 2024; Revised 25 March 2024; Accepted 25 December 2024; Published Online 15 April 2025.
DOI: 10.61091/jcmcc127a-253

to turn their eyes to renewable and clean energy such as solar energy, wind energy, biomass energy, etc. At this time, the DC power grid has received widespread attention by virtue of the advantages of high distributed energy consumption capacity [1-3]. On the basis of the original alternating current (AC) power grid, a layer of DC network is superimposed by DC transmission technology to form a hybrid AC-DC power system, thus establishing a super grid with wide-area interconnection of multiple energy sources [4-5]. The many advantages of hybrid AC/DC power distribution, especially the high consumption capacity of distributed energy, make it one of the important ways to solve the energy crisis [6-7]. Pooling distributed energy sources from all over the world, combining with the original AC grid, and constructing AC-DC hybrid grids is the development direction of the future power system [8-9].

The gap of multi-area protection coordination strategy limits the development of AC-DC hybrid power system. In the AC-DC hybrid power system, realizing the mutual coordination and cooperation between AC system and DC system is the key measure to maintain the safe operation of the system to realize the multi-area protection [10-12]. However, the special characteristics of AC/DC hybrid power distribution methods make their fault types and fault characteristics differ greatly from those of AC power distribution methods, and bring new difficulties for their fault protection [13-15].

Sarangi, S. et al. elucidated the specific advantages and barriers to the development of AC-DC hybrid power systems, which can provide uninterrupted and secure power at high load demands, but bidirectional tidal currents, low inertia, and transitions between different modes of operation are the challenges faced by AC-DC hybrid power system protection [16]. Shu, Y. et al. pointed out that the control performance of the traditional stability control system is reduced due to the strong coupling and renewable energy integration characteristics of the AC/DC grid, based on which the key issues and technologies in the construction of power system protection are analyzed to contribute to the construction of an integrated defense system for AC/DC hybrid power systems [17]. Abdelwanis, M. I. et al. introduced a neural network optimization approach for AC/DC hybrid microgrids, which identifies various challenges in hybrid power systems and proposes solutions to provide improved paths for the development of smart grids and distributed power system technologies, as compared to traditional microgrid structures [18]. Dahane, A. S. et al. investigated coordinated control schemes in the context of multi-objective control requirements for AC-DC hybrid power systems, categorized them into distributed, centralized, and decentralized control strategies, and discussed various aspects related to these control objectives and the advantages and limitations of their control strategies, respectively [19]. Wang, G. et al. designed a power coordinated control strategy based on step control theory to maintain the power stability of AC-DC hybrid microgrid, for lower control, multiple control modes are designed for converters in different application scenarios, and for higher control, a power coordinated control strategy is designed for grid-connected islanding mode, to achieve the effectiveness and stability of the microgrid under various operating conditions [20]. Prommetta, J. et al. showed that electromagnetic and electrical interactions between AC and DC lines affect AC protection and DC control, discussed fault detection and fault response for AC protection and DC control in a hybrid AC/DC overhead line project, and proposed a fault clearing method based on simulation experiments [21]. Qian, Z. et al. described the phenomenon of current surge faults in AC and DC distribution networks, for which a comprehensive control and protection strategy for AC and DC distribution networks is proposed, which is based on the principles of active current limiting control (ACLC) and single-ended fault identification and protection, and is able to effectively reduce the average rate of rise of the fault current through fast fault area identification [22]. Chen, Z. et al. established a mathematical optimization model for coordinated control in the steady-state security domain of an AC-DC hybrid power system by taking the minimum control cost as the objective function and combining dynamic constraints to solve the optimal efficiency control scheme for preventive and corrective control [23].

The study proposes and realizes an AC/DC distribution network trend calculation and network loss analysis method based on the alternating iteration method by using the power system trend distribution prediction method and different control strategies such as master-slave control and droop control. The study first adopts the method of power system trend distribution prediction, and proposes to realize an AC/DC hybrid distribution network trend calculation and network loss analysis method based on the alternating iteration method, to avoid the relay protection device misoperation in the case of system overload and fault, and to prejudge the faulty line in advance, in order to ensure that the adaptive relay protection can be correctly operated. Subsequently, combined with the real-time operating conditions of the power grid, the Agent reinforcement learning mechanism is introduced to enhance the adaptive ability of the multi-agent system, and the adaptive coordinated protection method based on the MAS power grid is proposed. Finally, the adaptive multi-agent system structure is combined with the traditional adaptive protection technology to realize the MAS adaptive current interruption protection, and simulation verification is carried out.

2. Trend calculation of AC/DC hybrid power systems

2.1. AC-DC hybrid distribution network topology and mathematical modeling

2.1.1. Research on hybrid AC/DC distribution network planning models and algorithms

1) Radial structure.The biggest advantage of radial DC distribution network is its simple structure and compatibility with AC distribution network. However, it has the same defects as the traditional AC radial network: the voltage level at the end of the line decreases with the increase of transmission distance and when a node fails, it will cause a large area of blackout. Therefore, this topology is only applicable to a small range of low-voltage distribution networks.

2) Two-terminal power supply structure.This topology is similar to the combination of two radial DC distribution networks, and the direction of the current is also fixed during normal operation. The essential difference between this topology and the radial distribution network is the improvement of power supply quality and reliability. The voltage level within the system is ensured by the dual power supply. In addition, when a fault occurs at any point in the system, the network can be converted to a single-power radial network to continue supplying power, reducing the area of outage and providing higher reliability of power supply. However, the construction cost of this network structure is higher, and it is suitable for medium and low voltage distribution networks.

3) Ring structure.This type of power supply has a higher reliability than the two-end power supply type DC distribution system, but also can make the load uniformly distributed in the DC sub-network, high system stability. When a fault occurs somewhere in the system, the relay protection device will locate and remove the fault. During this time, the ring network transforms into a two-end power supply type network to continue operation, ensuring that the non-faulted area is not affected. The disadvantages of this network structure are the further increase in construction costs and the higher requirements for relay protection, which are suitable for medium voltage distribution networks with higher voltages.

2.1.2. VSC steady state modeling. Since this paper focuses on solving the current calculation results of the AC-DC hybrid grid, the following assumptions are made about the converter in the analysis process:

1) The converter is a three-phase symmetrical structure;

2) The current and voltage are ideal waveforms;

3) The transient characteristics of the converter are not considered, and the phase change process is completed instantaneously.

In order to calculate the three-phase unbalanced current of VSC, this paper adopts the symmetrical component method to deal with the interface between the converter and the AC network. The voltage sequence component $U_{S(0,1,2)}$ and power sequence component $S_{S(0,1,2)}$ at the interface are:

$$\begin{cases} U_{s(0,1,2)} = T^{-1}U_s(a,b,c) \\ S_{s(0,1,2)} = T^{-1}S_s(a,b,c) \end{cases} \tag{1}$$

where T is the symmetric component transformation matrix with the expression:

$$T = \begin{bmatrix} 1 & 1 & 1 \\ \alpha^2 & \alpha & 1 \\ \alpha & \alpha^2 & 1 \end{bmatrix} \tag{2}$$

Where $\alpha = e^{j120}$

When the operation direction of the converter is transformed from AC sub-network to DC sub-network, the converter can be equated as an active element, and the voltage transformation takes the positive sequence component $U_{c(1)}$ after symmetrical transformation, which is related to the DC side voltage U_{dc} as:

$$\left|\dot{U}_{c(1)}\right| = \frac{\mu M}{\sqrt{2}} U_{dc} \tag{3}$$

Where, M is the modulation coefficient and μ is the modulation ratio.

The VSC will generate some losses during operation, which will have some impact on the results of the tidal current calculation. In this paper, the converter loss is taken into account in the calculation and the generalized converter loss model is used.

The loss model can be expressed as:

$$\begin{cases} P_{loss} = a + bI_{dc} + cI_{dc}^2 \\ I_{dc} = \dfrac{\sqrt{P_c^2 + Q_c^2}}{\sqrt{3}U_c} \end{cases} \tag{4}$$

Where P_{loss} is the converter loss; I_{dc} is the current on the DC side; P_c and Q_c are the active power and reactive power flowing into the converter on the AC side; coefficients a, b and c simulate the intrinsic loss of the converter, the loss linearly related to the current, and the loss squarely related to the current, respectively. The loss model is derived from the DC side of the converter, and the coefficients a, b, and c are empirical parameters that change with the system operation and converter parameters. On this basis, the current calculation also needs to satisfy the power conservation. Therefore the VSC currents should also satisfy:

$$P_s = P_z + P_c \tag{5}$$

$$P_c = P_{dc} + P_{los} \tag{6}$$

In Eq. (5) and Eq. (6): P_z is the active loss generated by the converter and the line, and P_{dc} is the active power injected into the DC side.

The VSC converter has the ability to decouple the AC side from the DC side, i.e., it can independently control active and reactive power. Its most basic control methods are mainly categorized into three: constant power control, constant voltage control and sag control.

2.1.3. Load and Distributed Power Modeling

1) Wind power output model.Wind power is one of the most widely used and commercially valuable distributed energy generation technologies, which can convert wind energy into electricity. The output power of wind turbine is mainly affected by the wind speed, and its probability density is usually represented by the two-parameter Weibull distribution in the current research:

$$f(v)=\left(\frac{k}{c}\right)\left(\frac{v}{c}\right)^{(k-1)}\exp\left[-\left(\frac{v}{c}\right)^{k}\right] \tag{7}$$

$$k=\left(\sigma_w/E_w\right)^{-1.086} \tag{8}$$

$$c=E_w/\Gamma(1+1/k) \tag{9}$$

Where v represents the wind speed at the hub of the impeller in the fan, k and c represent the shape parameter and scale parameter in the Weibull distribution, and σ_w and E_w represent the standard deviation and the mean value, respectively.

The segmentation function of its active power is:

$$P_W(v)=\begin{cases} 0 & 0\le v\le v_d \\ P_r\left(v-v_{di}\right)/\left(v_{cr}-v_{ci}\right) & v_{ci}<v\le v_\sigma \\ P_r & v_{c\sigma}<v\le v_{co} \\ 0 & v>v_{co}\end{cases} \tag{10}$$

Where v_{cl} represents the cut-in wind speed, v_{cr} represents the rated wind speed, v_{co} represents the cut-out wind speed, and P_r represents the rated output power of the wind turbine.

When the wind turbine uses constant power factor control, the reactive power output Q_W of the wind turbine is:

$$Q_w=-P_w\tan(\arccos\theta) \tag{11}$$

Where, $\cos\theta$ denotes the power factor of the WTG.

2) Photovoltaic power generation output model.Solar energy is the most abundant energy on the earth, PV generator can convert light energy into electricity, and its core part is PV cell. The output power of PV generator is affected by the light intensity, there is a certain degree of volatility, the current study usually uses beta distribution to represent the probability density of light intensity over a period of time:

$$f(H)=\frac{\Gamma(\alpha+\beta)}{\Gamma(\alpha)\Gamma(\beta)}\left(\frac{H}{H_{\max}}\right)^{\alpha-1}\left(1-\frac{H}{H_{\max}}\right)^{\beta-1} \tag{12}$$

where H denotes the light intensity and Γ is the Gamma function; α and β denote the two shape parameters of the Beta distribution, respectively, whose values are calculated from the mean μ and variance σ of the light intensity over a period of time:

$$\alpha=\mu\cdot\left[\frac{\mu(1-\mu)}{\sigma^2}-1\right] \tag{13}$$

$$\beta=(1-\mu)\cdot\left[\frac{\mu(1-\mu)}{\sigma^2}-1\right] \tag{14}$$

Its output power function is:

$$P_p=\begin{cases} P_{px}\dfrac{H}{H_r} & H\le H_r \\ P_{px} & H>H_r\end{cases} \tag{15}$$

Where P_P represents the rated output power of the PV generator and H_r represents the rated light intensity.

3). Load modeling.There is often a certain error between the actual load in the power system and the predicted load, so it is not possible to use deterministic methods for system planning. Therefore, this paper uses normal distribution to represent the uncertainty of load:

$$P_{L,i} \sim N\left(\mu_{p,i}, \sigma_{p,i}^2\right) \tag{16}$$

$$Q_{L,i} \sim N\left(\mu_{q,i}, \sigma_{q,i}^2\right) \tag{17}$$

where $P_{L,i}$ and $Q_{L,i}$ denote the random quantities of nodal active and reactive loads, respectively; $\mu_{p,i}$ and $\mu_{q,i}$ denote the expectations of nodal active and reactive loads, respectively; and $\sigma_{p,i}^2$ and $\sigma_{q,i}^2$ denote the deviations of nodal active and reactive loads, respectively.

2.2. Design of tidal current algorithm based on alternating solution method

2.2.1. Methods for calculating system currents on the a.c. side.The AC side of the AC DC system can be calculated by the Newton-Raphson method. The traditional Newton-Raphson method mainly involves the Taylor series expansion of the tidal equation $F(X)=0$ and the omission of higher-order terms above the second order, and then solves it [24]. The essence of this method is that the central idea of the solution process is to continuously approximate the tidal solution using the modified equation through successive linearizations. The format of its iterations is:

$$\begin{cases} F\left(X^{(k)}\right) = -J^{(k)} \Delta X^{(k)} \\ X^{(k+1)} = X^{(k)} + \Delta X^{(k)} \end{cases} \tag{18}$$

where: X and ΔX are n-dimensional column vectors consisting of the n state variables and their corrections, respectively; $F(X)$ is a n-dimensional column vector containing the n functions; J is the Jacobi matrix, with his j th column element $J_{ij} = \frac{\partial f_i}{\partial x_j}$ in row i; the upper corner label k represents that each element in the J matrix takes its value at point $\left(X_1^{(k)}, X_2^{(k)}, \cdots, X_n^{(k)}\right)$.

2.2.2. Methods for calculating DC side system currents.When the AC and DC systems use the alternate solution method for trend calculation, the AC system and DC system can be solved separately. At this time, any one of the effective tidal current algorithms can be used on the DC side, and when the DC distribution system is an open-loop radial network or only a weak ring network structure exists, the forward back generation method with a relatively high computation rate can be used for the tidal current calculation.

The incoming branch of bus k of a DC distribution network is called branch k and the conductance matrix can be expressed as Y_k. The conductance matrix Y_k relates the currents at the ends of the branch to the bus voltage.

$$Y_k = \begin{vmatrix} Y_k^{11} & Y_k^{12} \\ Y_k^{21} & Y_k^{22} \end{vmatrix} \tag{19}$$

$$\begin{vmatrix} I_k \\ I_k' \end{vmatrix} = Y_k \begin{vmatrix} U_{k-1} \\ U_k \end{vmatrix} \tag{20}$$

Where: U_k and $U_k - 1$ represent the voltage of bus k and $k-1$ respectively; I_k represents the outgoing current of bus $k-1$; I_k' represents the incoming current of bus k.

The specific steps of the back generation process in DC system current calculation are as follows:

1) In the iterative step of the back generation process, the injected current is obtained from the DC voltage U_k of bus k with the load on the bus with DG, etc.: I_{Lk}, I_{Dk}.

2) From the obtained I_{Lk}, I_{Dk} and the outgoing branch current I_{k+1} of bus k, calculate the incoming branch current I'_k of bus k based on KCL.

$$I'_k = I_{Lk} + I_{Dk} - \sum_{j \in A_k} I_j - I_{k+1} \tag{21}$$

Where: A_k is the set of buses directly connected to bus k.

3) Calculate the voltage vector U_{k-1} for bus $k-1$ from U_k and the obtained I'_k.

$$U_{k-1} = \left(Y_k^{12}\right)^{-1} I'_k - Y_k^{22} U_k \tag{22}$$

4) From the obtained voltage $U_k - 1$ at bus $k-1$ and voltage U_k at bus k and the incoming branch current I'_k, calculate the outgoing branch current I_k at bus $k-1$.

$$I_k = Y_k^{11} U_{k-1} + Y_k^{22} U_k \tag{23}$$

The specific steps of the forward process in DC system current calculation are as follows:

1) From the voltage value U_{k-1} at bus $k-1$ and the outgoing branch current I_k, find the voltage U_k at bus k.

$$U_k = \left(Y_k^{12}\right)^{-1} I_k - Y_k^{11} U_{k-1} \tag{24}$$

2) Calculate the incoming branch current I'_k of bus k from the voltage U_{k-1} outgoing branch current I_k of bus $k-1$ and the obtained U_k in the process of back generation.

$$I'_k = Y_k^{21} U_{k-1} + Y_k^{22} U_k \tag{25}$$

3) Calculate the load and DG current injections from the obtained U_k: I_{LK}, I_{DK}; then calculate the outgoing branch current I_{k+1} of bus k from KCL.

2.2.3. Calculation method of network loss of AC/DC distribution network.The loss of AC and DC distribution network consists of three parts: AC side loss, converter loss and DC side loss, which can be calculated by equation (26).

$$P_{loss} = P_{ac-loss} + P_{vsc-loss} + P_{dc-loss} \tag{26}$$

Where: P_{loss} represents the total network loss of the system, $P_{ac-loss}$ represents the loss on the AC side of the system, $P_{vsc-loss}$ represents the converter operation loss, and $P_{dc-loss}$ represents the loss on the DC side of the system.

The loss on the AC side of the system $P_{ac-loss}$ can be calculated by the following equation:

$$\begin{aligned} P_{ac-loss} = \sum_{i=1}^{N} \sum_{i=1}^{N} \Bigg[& \frac{r_{ij}}{UU_j} \cos \delta_{ij} \left(P_{aci} P_{acj} - Q_{aci} Q_{acj} \right) \\ & + \frac{r_{ij}}{U_i U_j} \sin \delta_{ij} \left(Q_{ai} P_{acj} - P_{aci} Q_{acj} \right) \Bigg] \end{aligned} \tag{27}$$

Where: N indicates the number of nodes in the AC network; δ_{ij} indicates the difference in voltage phase angle between nodes i and j; r_{ij} indicates the resistance between nodes i and j.

For the network loss of the DC system there is no reactive power, so the network loss is calculated as the sum of the active power injected into the nodes on the DC side of each converter and the power injected into the DER equipment, and then the DC load can be removed:

$$P_{dc-loss} = \sum_{i=1}^{n} P_{vSC.dci} - \sum_{j=1}^{m} P_{dcj} + \sum_{z=1}^{p} P_{DER.dcz} \tag{28}$$

Where: $P_{VSC,dci}$ denotes the injected power on the DC side of the ind converter, P_{dcj} denotes the operating power of the jth load, and $P_{DER,dcz}$ denotes the injected power of the zth DER device.

2.3. Example analysis

Example 1: Take a typical medium voltage AC/DC hybrid distribution network abstracted from an actual distribution network in a region as an example, where the IEEE33 nodes are subordinate parts of the AC distribution network. Specifically, they are selected from the first 27 AC nodes and named 48 to 74, which are attributed to AC distribution partition II. In addition, these two will be connected to each other through a multi-terminal DC distribution technology to form an AC double-feeder interconnection system that combines the characteristics of radial, two-terminal and multi-terminal DC distribution grids. Experiments are carried out using simulation software and the convergence accuracy is found to be minimum 0.000001.The experiments are analyzed using 1MVA as standard capacity. The example system is shown in Fig. 1.

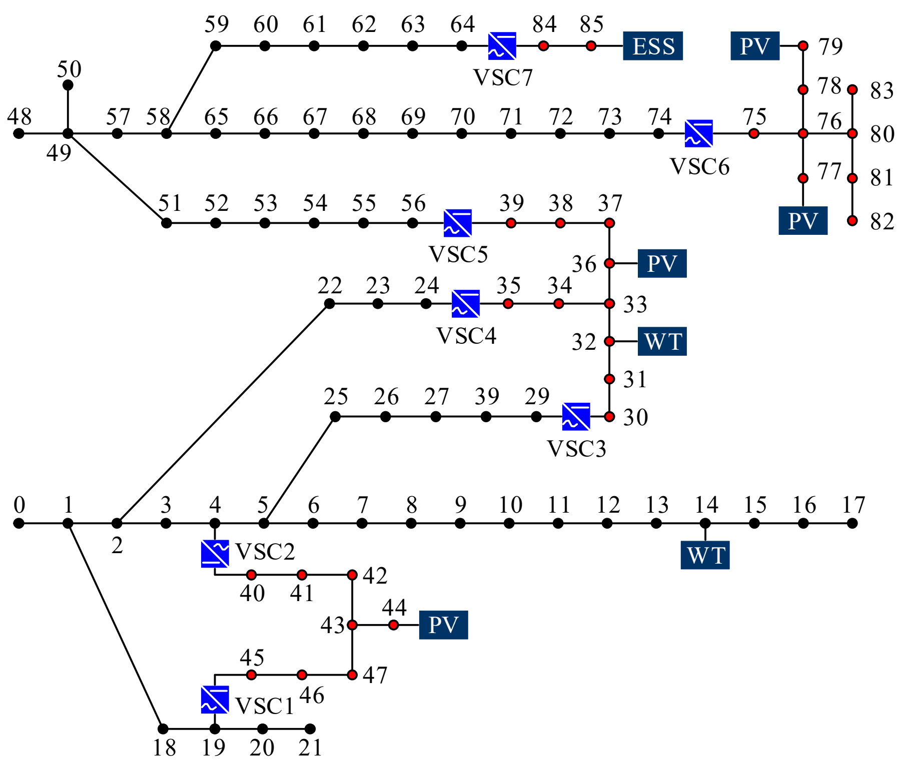

Fig. 1. AC-DC power distribution system calculation case system

The example system is connected to the converters at nodes 4, 19, 24, 29, 56, 64, and 74 to form a two-terminal DC distribution network using a droop control strategy (nodes 4 and 19) and a multi-terminal DC distribution network using a master-slave control strategy (nodes 24, 29, and 56), respectively.

A photovoltaic (PV) power plant is incorporated at node 44, with a wind turbine and PV installed at each of the 32 and 36 facilities. The addition of energy storage equipment at node 84 makes the overall operation normal.

The radial DC distribution grid is connected at node 74 by optimizing the operating power of the converter. In addition, the PV plant is also connected to DC nodes 77 and 79, respectively. The DC side of this converter has a voltage of 10 kV and uses U as its voltage range.

The DER equipment and related parameters in the AC/DC distribution system are shown in Table 1, while Table 2 shows the related parameters of the converter. In addition, Table 3 shows the operating loss data. The results from the DC side current calculation are shown in Table 4, and Table 5 shows the results from the AC side current calculation. A total of five iterative steps are used.

Table 1. Parametric design

Node position	85	79	77	44	36	32	14
Capacity	100	200	200	200	300	300	200

Table 2. VSC parameters

VSC number	1	2	3	4	5	6	7
Power /KW	1.031	1.031	0.679	0.679	0.955	2.522	0.247

Table 3. Running loss

Alternating current loss /kw	Converter loss /MW	Dc side loss /MW	Distribution loss /MW
0.5088	0.2095	0.0571	0.9045

Table 4. Current calculation of dc system

Node number	Voltage amplitude /p.u.	Active load /k W
30	1	
31	0.982	200
32	0.98	50.0013
33	0.976	210
34	0.976	290
35	0.98	240
36	0.975	170
37	0.979	210
38	0.977	250
39	0.981	110
40	0.998	190
41	0.982	220
42	0.978	270
43	0.975	150
44	0.975	90
45	0.988	190
46	0.98	220
47	0.978	270
75	0.986	230
76	0.978	140
77	0.979	250
78	0.98	260
79	0.977	190
80	0.972	150
81	0.976	390
82	0.971	230
84	1.002	190
85	1	230

Table 5. The results of the communication system flow

Node number	Voltage amplitude /p.u.	Angle /(°)	Node load	
			Active load /kw	Reactive load /kw
0	1	0	-	-
1	0.989	0.074	100	50
2	0.98	0.114	80	40
3	0.986	0.014	110	70
4	0.982	0.004	50	35
5	0.982	0.054	50	20
6	0.982	-0.154	210	100
7	0.983	-0.024	210	100
8	0.986	-0.026	50	20
9	0.986	0.014	50	20
10	0.985	0.124	43	35
11	0.939	0.141	50	40
12	0.945	0.234	50	40
13	0.928	0.274	110	80
14	0.931	0.261	400	10
15	0.958	0.260	50	25
16	0.951	0.109	50	25
17	0.947	0.148	80	45
18	0.982	-0.021	80	45
19	0.983	-0.517	80	45
20	0.988	-0.572	80	45
21	0.953	-0.516	410	45
22	0.983	0.184	410	50
23	0.992	-0.234	50	200
24	0.962	-0.034	50	200
25	0.984	0.054	110	27
26	0.946	-0.044	200	20
27	0.933	-0.076	100	70
28	0.935	-0.194	200	600
29	0.915	-0.151	100	50
48	1.001	0	-	-
49	0.982	0.084	131.45	102.12
50	0.981	0.056	11.43	14.72
51	0.979	0.004	35.27	27.43
52	0.984	0.044	69.11	60.23
53	0.981	-0.054	141.61	65.24
54	0.984	-0.074	103.42	60.32
55	0.986	-0.016	27.33	14.24
56	0.985	-0.054	80.51	55.11
57	0.985	-0.094	182.21	101.33
58	0.983	-0.114	141.23	71.25
59	0.983	-0.124	21.01	16.45
60	0.945	-0.411	55.21	21.42
61	0.979	-0.584	142.27	114.45

62	0.982	-0.654	24.27	27.55
63	0.982	-0.656	35.44	22.36
64	0.984	-0.784	32.11	22.12
65	0.984	-0.504	26.35	10.73
66	0.987	-0.752	154.53	70.27
67	0.979	-0.224	543.15	349.73
68	0.982	-0.878	181.52	167.28
69	0.982	-0.924	91.47	53.13
70	0.985	-1.174	80.24	35.21
71	0.941	-1.006	163.69	96.83

In order to verify the effectiveness of the AC and DC algorithms, taking AC partition one as an example, without loss of generality, the value of the current data on the AC side of the converter can be derived using the AC current calculation method, and the DC current data after the converter and the converter can be equated to a PQ node. And the equivalent PQ node current data is substituted into the traditional AC current calculation for verification and validation, and the results are shown in Figure 2. From the figure, it can be seen that the two curves completely overlap in the range of 0~30 nodes, which proves the effectiveness and accuracy of the AC/DC hybrid distribution network current algorithm based on the alternating iteration method proposed in this paper.

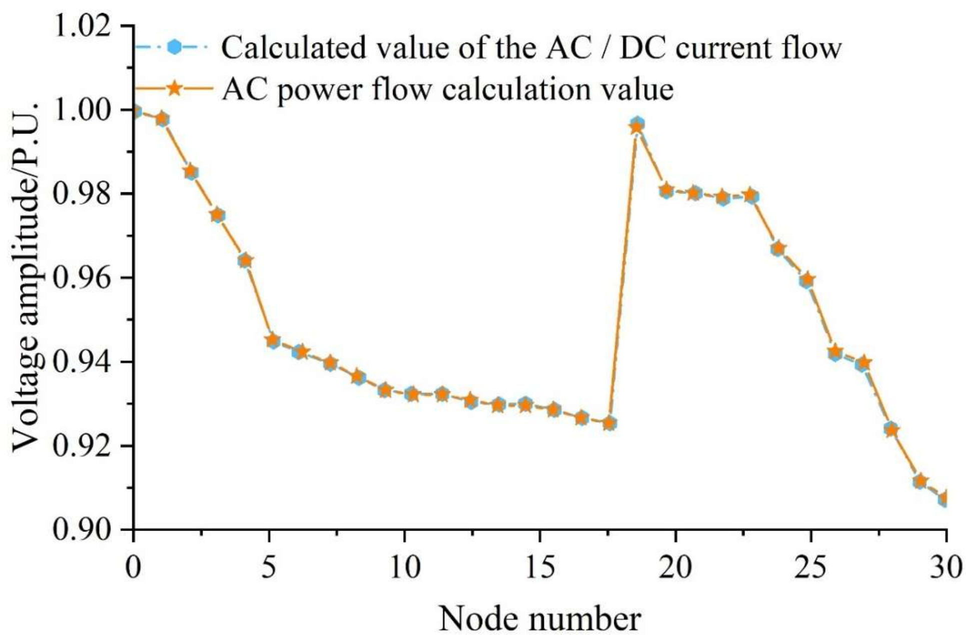

Fig. 2. Ac partition a node voltage value

Example 2: In the classical IEEE33 node, DC lines and distributed power sources are added as an improved example. The simulation structure of AC/DC hybrid distribution network is shown in Fig. 3. ① As the voltage level of the DC grid, 12 kV is taken. ② VSCI implements constant DC voltage control; while VSC2 relies on constant AC power for adjustment. ③ Tables 6 and 7 show the electrical parameters of each node in this optimization scheme such as the line resistance and the load information carried by the node. ④ The powers of the four distributed generators are 150 kW, 250 kW, 80 kW and 100 kW. The AC reference voltage UB = 12.66 kV and the power reference value SB = 10 MVA is selected.

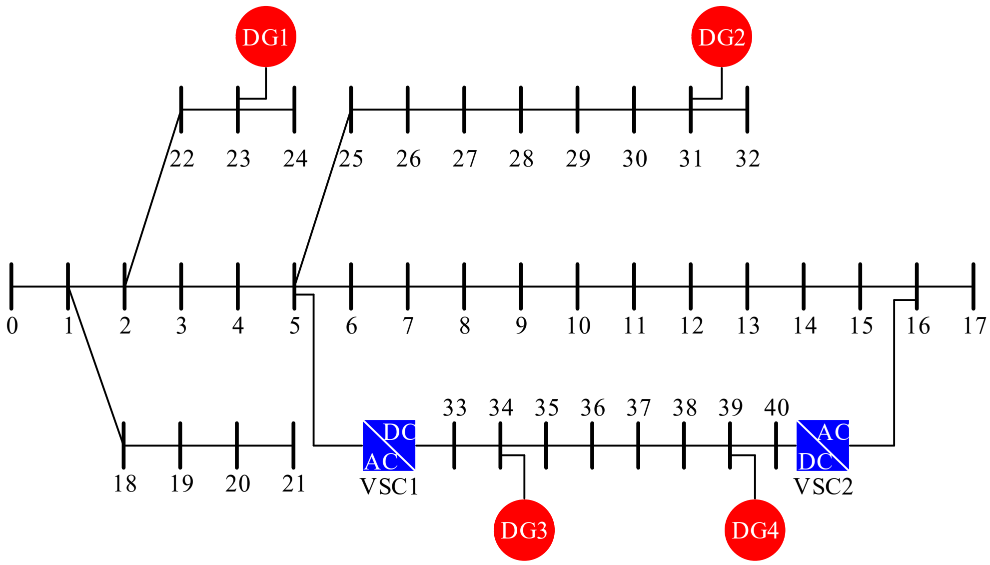

Fig. 3. Simulation case of AC / DC hybrid distribution network

Table 6. Branch resistance of the DC system

Branch circuit	Resistance/ Ω	Branch circuit	Resistance/ Ω
33-34	0.3742	37-48	0.4325
34-35	0.6072	38-39	0.7257
35-36	0.5276	39-40	0.5769
36-37	0.7349		

Table 7. The DC system p-node parameters

Node type	Node number	Load power /kW	Node number	Load power /kW
P node	34	40.26	38	58.97
	35	50.55	39	297.14
	36	45.09	40	35.28
	37	71.27		

In the VSC equivalent model, since the resistance is much smaller compared to the reactance, the resistive characteristics of the VSC are not considered in general studies. In this paper, in order to account for the losses of the VSC, the resistance of the existing line can be multiplied by 0.1-0.2 as the equivalent resistance of the converter, and then multiplied by 5-10 as its corresponding equivalent reactance. It is further assumed that the impedance of the VSCl equivalent model is set to 0.1256 + j0.8792 Ω, and the impedance of the VSC2 equivalent model is set to 0.0916 + j0.7328 Ω. Assuming that the power injected into the AC portion of the VSC2 equivalent model is 70+j80kVA, the following simulation results can be obtained by performing the current simulation simulation.

Fig. 4-Fig. 6 show the voltages in each quadrant of the AC network nodes, respectively, and the results show that no matter whether the voltage at node 1 is at 1 or 0, the final voltage gradually smoothes out with the node. Table 8 shows the voltage information of each node on the DC network, from the table it can be seen that from the beginning of the voltage of 1.0000 to the last 0.9684, the overall trend is decreasing.

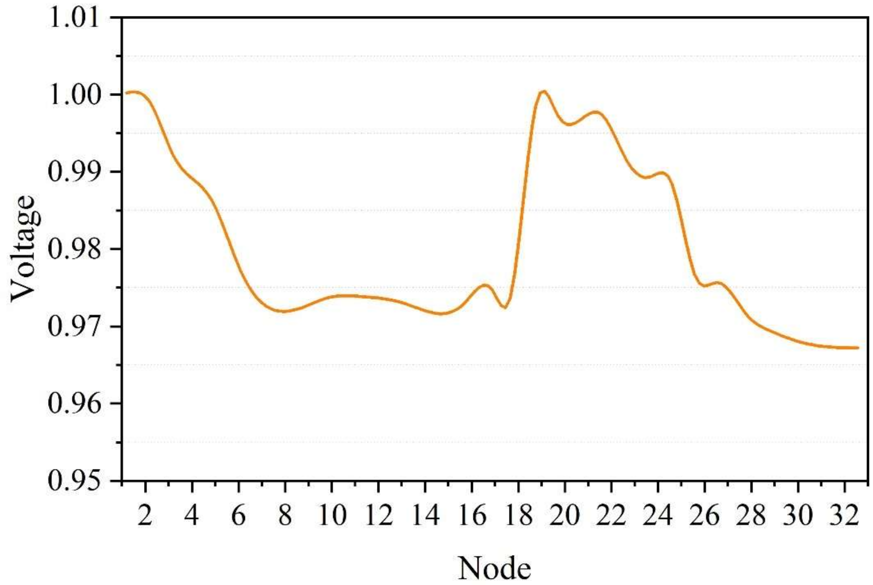

Fig. 4. A-phase node voltage of the AC-DC hybrid distribution network

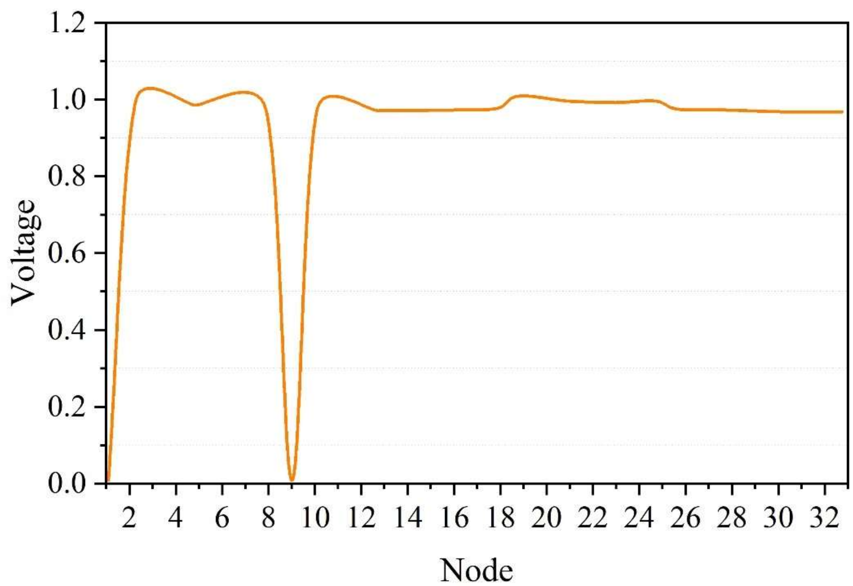

Fig. 5. B-phase node voltage of AC-DC distribution hybrid grid

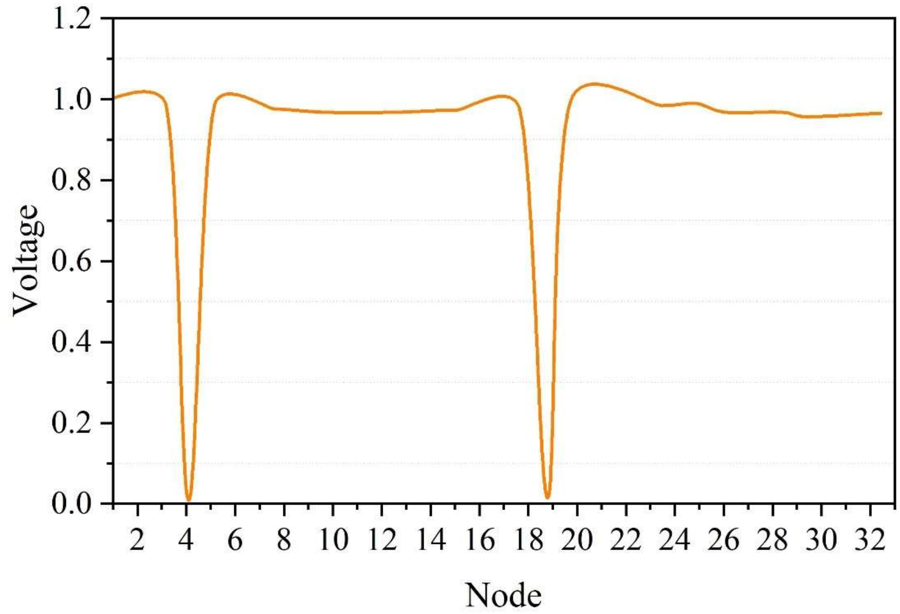

Fig. 6. The c-phase node voltage of the AC-DC hybrid distribution network

Table 8. Simulation results: DC node voltage

Node number	Node voltage /p.u.	Node number	Node voltage /p.u.
33	1.0000	37	0.9722
34	0.9764	38	0.9712
35	0.9742	39	0.9708
36	0.9735	40	0.9684

3. MAS-based adaptive multi-region protection coordination strategy

3.1. Organizational structure of MAS

3.1.1. Networked structure.This structure is a flat structure where the relationship between Agents is equal. The distinctive features of this structure are information localization and peer-to-peer communication, therefore, some scholars also call it a distributed autonomous structure. Each Agent in the system is autonomous and independent. When the task is beyond the scope of its own ability, Agent can interact and cooperate with other, and each Agent communicates directly with each other, regardless of the distance. It is a horizontal structure.

This structure best reflects the characteristics of multi-agent, and early applications of networked structure include the proposed networked market structure and the proposed networked expert group structure. However, the network structure requires direct communication between each agent in the system, and needs to save a huge amount of information, especially when the system structure is large and complex, the number of communication links of each agent in the system will be particularly large, which will lead to a significant reduction in the efficiency of the system.

3.1.2. Hierarchical structure.Each Agent in the hierarchical structure is divided into layers, and the relationship between them is no longer equal, and the hierarchical relationship is fixed. The decision-making and control power of each layer is concentrated in the Agent of the upper layer, which is responsible for controlling and coordinating the behavior of the Agent of the lower layer, and the communication between the Agents of the same layer has to go through the upper layer, which is also responsible for storing the relevant information of the Agent of the lower layer. The communication of this structure is obviously not as simple as the network structure.The MAS structure is shown in Fig.

7, the lowest layer is the field Agent layer, the middle layer is the coordination Agent layer, and the top layer is the decision-making Agent layer. In this structure, each Agent layer only needs to save the information of its corresponding lower Agent layer, which has the advantage of information storage compared to the network structure, but its communication method is a bit complicated compared to it, especially when the amount of information interacted by each layer is relatively large, and it is easy to encounter the bottleneck problem.

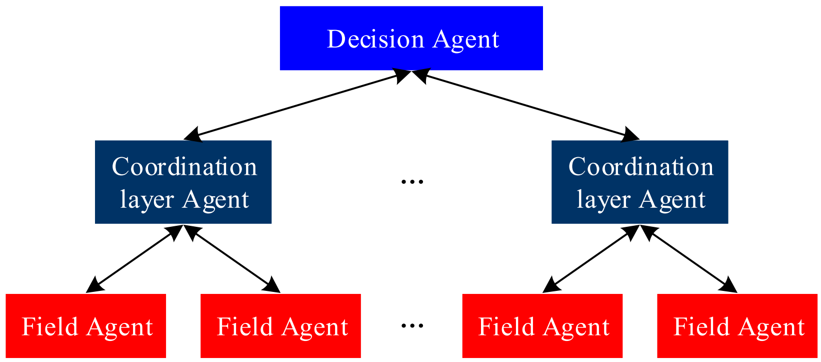

Fig. 7. The hierarchical structure of the MAS

3.1.3. Unionized structures.As the system is getting larger and more complex in size and structure, the number of Agents is increasing, and how to solve the information interaction between them will become a key issue in the establishment. For this reason, some scholars have proposed the idea of coalitional structure. The basic idea is to divide each Agent in the MAS into small coalitions composed of appropriate numbers according to some relationship (distance or structure, etc.). The whole system consists of these different small coalitions, and each small coalition has a coalition Agent called Facilitator, which acts as a transit organization between the small coalitions and is mainly responsible for providing services for the interaction of the small coalitions.

3.2. Coordinated Protection Architecture for Multi-Agent Systems

3.2.1. Adaptive Agent Based on Reinforcement Learning.The adaptive Agent operation system based on reinforcement learning mainly includes the adaptive Agent, the role and the external environment, in which the adaptive Agent mainly consists of four parts, namely, the perception module, the decision-making module, the behavior pool and the execution module [25].

1) The perception module is the Agent's perceptron, which is responsible for sensing the state changes of the external environment, transferring the results of its perception to the decision-making unit, and forwarding the tried-and-true environment evaluation to the learner.

2) Decision module consists of three units: learner, knowledge and adaptive strategy. The learner implements the adaptive Agent to learn the effects obtained from the operations it performs through some learning algorithm; the learned knowledge will be stored in the knowledge unit; the adaptive strategy unit encapsulates the behaviors that the adaptive Agent can perform and specifies the mapping relationship between the external perception and the adaptive actions, which is strengthened or weakened in the learning.

3) Behavior pool is mainly to cache the behavioral state of the Agent, and the behaviors in the behavior pool are realized to be called by the decision module and finally executed by the execution module to act on the environment.

4) The execution module is the effector of the Agent, which executes the specific behaviors in the behavior pool and acts on the external environment, prompting the environment state to change.

When the perceptron perceives a new change in the environment, it will trigger a new round of "perception-decision and learning-execution" process.

3.2.2. Hierarchical Multi-Agent System Protection Architecture.This paper adopts hierarchical structure applied to multi-agent system design. From the substation point of view, each interval-oriented protection in the substation adopts distributed information acquisition and control mode, and the information collection and decision-making processing of the station level protection adopts centralized mode; from the perspective of regional relay protection composition, the station level protection of each substation adopts distributed mode, and the wide-area protection decision-making center adopts centralized mode. The hierarchical multi-agent system protection structure fully embodies the advantages of the combination of distributed and centralized, effectively solving the shortcomings of the traditional purely distributed system with a large amount of information in the network, but a small amount of information accessed by a single decision-making center, as well as the traditional centralized decision-making center with an excessive amount of information in the communication.

3.3. MAS Adaptive Multi-Area Current Disconnect Protection Coordination

3.3.1. Conventional current interruption protection.Current protection which operates immediately as a result of an increase in current when both reliability and selectivity are met is known as time-limited current-break protection. In order to ensure the correct selectivity of the action, the time limitless current interruption protection can only protect part of the line. The time-limitless current interruption protection is also known as section I current protection, and the protection device is located on the power supply side of each line of a single-side power supply radial grid.

When a power system is analyzed for a short circuit, if the power supply potential is certain, the value of the short-circuit current I_K depends on the fault type factor K_K and the total reactance X_Σ between the short-circuit point and the power supply (ignoring the total resistance R_Σ), and can generally be expressed as:

$$I_K = \frac{K_K E_{ph}}{X_\Sigma} = \frac{K_K E_{ph}}{X_s + X_1 l} \tag{29}$$

Where: K_K : Coefficient of short-circuit fault type, in case of two-phase short-circuit, $K_K = \sqrt{3}/2$; in case of three-phase short-circuit, $K_K = 1$.

E_{ph} : Phase potential of the equivalent power supply of the system (V).

X_s : Equivalent reactance of the system normalized to the protection installation (Ω).

X_1 : Positive sequence reactance of the line per unit kilometer length (Ω / km).

l: Distance from the short-circuit point to the protection installation (km).

Suppose that protection 1 and protection 2 are installed in lines WL1 and WL2 respectively. According to the requirement of selectivity, when a short-circuit fault occurs in the adjacent next-level line, the protection device does not start; for protection 1, when a short-circuit occurs at point K2 at the first end of the line WL2, protection 1 does not act, and protection 2 should act to remove the short-circuit fault. As the maximum short-circuit current at point K2 and the maximum short-circuit current at the short-circuit on bus B at the end of WL1 of this level of line are approximately equal, the action current of protection 1 shall be greater than the maximum operation mode for:

$$\begin{aligned} I_{op,1}^{t} &> I_{kB\max}^{(3)} \\ I_{op,1}^{l} &= K_{rel}^{I} I_{k\max}^{(3)} \end{aligned} \tag{30}$$

Where $I_{op,1}^{I}$: Protective device 1, paragraph I current protection action current value, also known as the protective device primary action current:

K_{rel}^{I}: Reliability coefficient of current protection paragraph I. When the DL electromagnetic type current relay is used, the value is 1.2-1.3; when the GL inductive relay is used, the value is 1.5-1.6.

$I_{kB\max}^{(3)}$: RMS value of the cycle component of the primary transient short-circuit current during a three-phase short-circuit on busbar at the end of line B under the maximum operation mode of the system.

The Protection Regulation requires a calibration sensitivity factor of 15%-20% for a two-phase short-circuit in the minimum mode of operation, and $m \geq 50\%$ in the maximum mode of operation. The protection ranges are as follows:

$$\begin{cases} l_{p,\min} = \dfrac{1}{X_1}\left(\dfrac{\sqrt{3}}{2}\dfrac{E_{ph}}{I_{op,1}^{I}} - X_{s,\max}\right) \\ l_{p,\max} = \dfrac{1}{X_1}\left(\dfrac{\sqrt{3}}{2}\dfrac{E_{ph}}{I_{op,1}^{I}} - X_{s,\min}\right) \end{cases} \tag{31}$$

3.3.2. Adaptive flow rate cut-off protection.The time-less current interruption protection can only protect part of the length of this line, for this reason, adaptive current interruption protection is proposed. Adaptive relay protection is characterized by a timely change in the operating characteristics or setting value of the protective device according to the power system operation mode and the occurrence of different types of faults. The current-flow interruption protection selects the action current setting value according to the maximum operation, i.e:

$$I_{op,1}^{I} = K_{rel}^{I} I_{k,\max} = \frac{K_{rel}^{I} K_K E_{ph}}{Z_{s,\min} + Z_L} \tag{32}$$

Where: $Z_{s,\min}$: Minimum impedance of the equivalent positive sequence of the system.

Z_L: Positive sequence impedance of the protected line.

E_{ph}: System equivalent phase potential, constant.

K_{rel}^{I}: Reliability factor.

K_K: Short circuit type factor.

System operation mode, short-circuit type coefficient K_K and the short-circuit point in the protected line location determines the size of the protection current, located in line αZ_L at the short-circuit, the short-circuit current is:

$$I_k = \frac{K_k E_{ph}}{Z_s + \alpha Z_L} \tag{33}$$

Making Eq. (32) and Eq. (33) equal, the current flow protection range α can be found to be:

$$\alpha = \frac{K_k\left(Z_{s,\min} + Z_L\right) - K_{rel}^{I} Z_s}{K_{rel}^{I} Z_L} \tag{34}$$

Eqs. $K_{rel}^{I} > 1$, $K_k \leq 1$, $Z_s > Z_{s,\min}$, so that the protection range in the maximum mode of operation is greater than the actual protection range α, and the protection range will be shortened to zero as the short-circuit type factor K_K becomes smaller and Z_s increases. The condition for the protection range to be zero is:

$$Z_s = \frac{K_k}{K_{rel}^{I}}\left(Z_{s,\min} + Z_L\right) \tag{35}$$

To overcome the shortcomings of Eq. (32), the adaptive current interruption protection current is set to:

$$I_{op,1.x} = \frac{K_{rel}^{I} K_{K} E_{ph}}{Z_{s} + Z_{L}} \tag{36}$$

Where: Z_s Equivalent positive sequence impedance of the system at the protection installation, which varies according to the mode of operation. The adaptive current break protection range is:

$$\alpha_{s} = \frac{Z_{L} - \left(K_{rel}^{I} - 1\right) Z_{s}}{K_{rel}^{I} Z_{L}} \tag{37}$$

From equation (37), it can be seen that α_s varies with the change of system impedance Z_s, but always meets the basic requirements of current flow protection and is in an optimal state. The condition that the adaptive protection range is zero is:

$$Z_{s} = \frac{Z_{L}}{K_{rel}^{I} - 1} \tag{38}$$

Comparison from Eq. (34) and Eq. (37) can be made:

$$\alpha_{s} = \frac{\left(Z_{L} + Z_{s} - K_{rel}^{I} Z_{s}\right)}{K_{k}\left(Z_{L} + Z_{s,\min}\right) - K_{rel}^{I} Z_{s}} \alpha \tag{39}$$

3.3.3. MAS Adaptive Current Disconnect Protection.The MAS protection system contains several Agent units, each of which collaborates with each other to accomplish the protection task. The protection Agent is composed of several algorithm modules, which are called by the system according to the real-time operation. The adaptive current interruption protection algorithm also belongs to the protection Agent algorithm module for the protection Agent to choose to call. First, the execution Agent group collects data from the power system and passes the collected information to the coordination Agent group. Secondly, the coordinating Agent group checks the collected information and calculates the change of fault components and system operation status, and transmits the calculation results to the scheduling Agent group and the protection Agent. Again, the scheduling Agent group makes adjustments based on the results and sends the instructions back to each relevant coordinating Agent group, and detects the operating status of the coordinating Agent group. The Protection Agent judges the fault type and phase according to the detected value, selects the corresponding protection module, gives the protection action to the Execution Agent group, and finally the Execution Agent group handles the fault. MAS adaptive coordinated protection system organically combines the MAS system with the adaptive protection system, utilizing the characteristics of multi-agent system hierarchical partitioning, which makes the protection ability improved, while maintaining the normal operation of the power grid.

4. MAS Adaptive Multi-Regional Protection Coordination Simulation Analysis

4.1. Impact of the point of failure

When the power potential ratio h is 0.93 and the potential difference δ is 20º, the location of the fault point is divided into 5, which are at the first end, at the 1/4 point, at the center point, at the 3/4 point, and at the end. Figure 8 shows the trajectory of the measured resistance R_{am}, from which it can be clearly seen that R_{am} increases with R_g, and the closer it is to the N section, the larger R_{am} is, with a maximum value of 160. Figure 9 shows the trajectory of the measured reactance X_{am} at different locations on the line. The horizontal coordinate represents R_g and the vertical coordinate represents X_{am}, and the overall reactance shows an increasing trend.

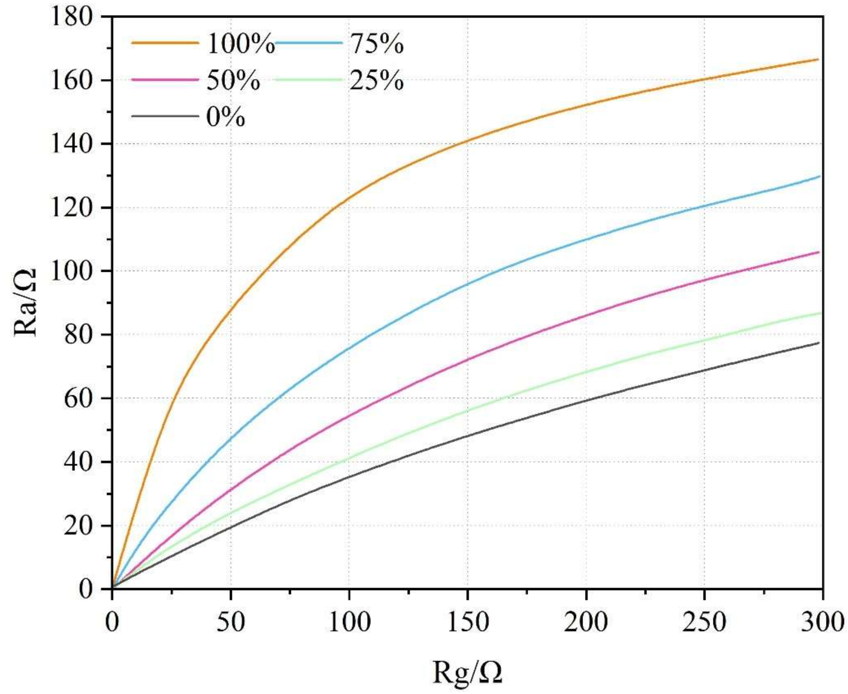

Fig. 8. Resistance changes were measured at different fault points

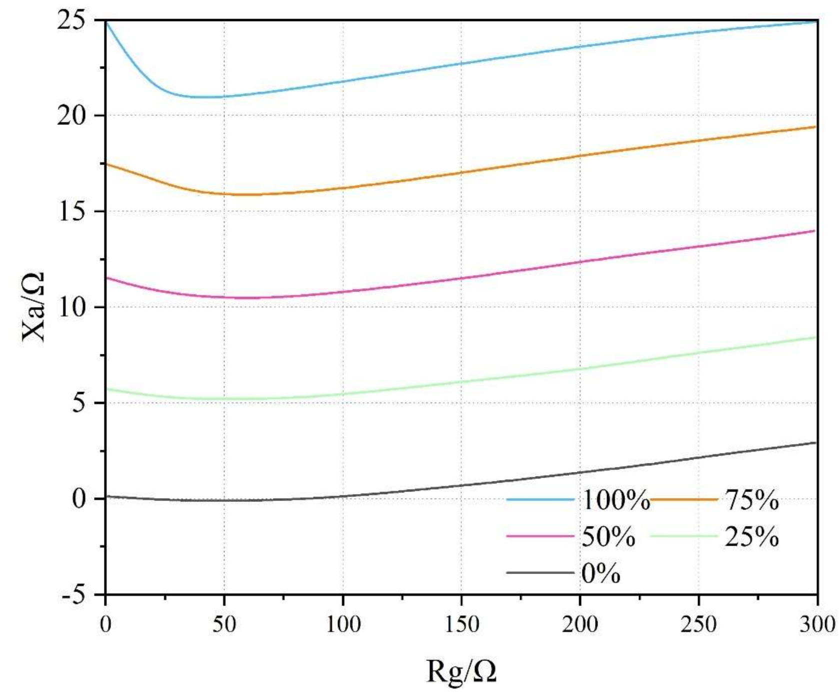

Fig. 9. The change trajectory of the reactance is measured at different fault points

4.2. Multi-Agent Based Adaptive Action Characterization

The system parameters are unchanged, and the trajectory of the measured impedance Z_{am} changes nonlinearly when R_g and the location of the fault point change, and the measurement results are shown in Fig. 10. Line Ⅰ in the figure indicates the trajectory of the change of each point of Z_{am} in the case of no transition resistance. From the figure, we can see that Z_{am} is only related to the location where the short circuit occurs, and its trajectory is a straight line perpendicular to the x-axis. Line II shows the relationship between R_{am} and X_{am} when a short circuit occurs at 90% of the line and at the same time R_g changes. Line Ⅲ shows the trajectory of Z_{am} change from 0% to 90% of the short-circuit point when R_g =280 Ω. Line Ⅳ indicates the R_g change from 0% to 280 Ω. The area enclosed by the four lines Ⅰ, Ⅱ, Ⅲ and Ⅳ indicates the operating area of the impedance relay.

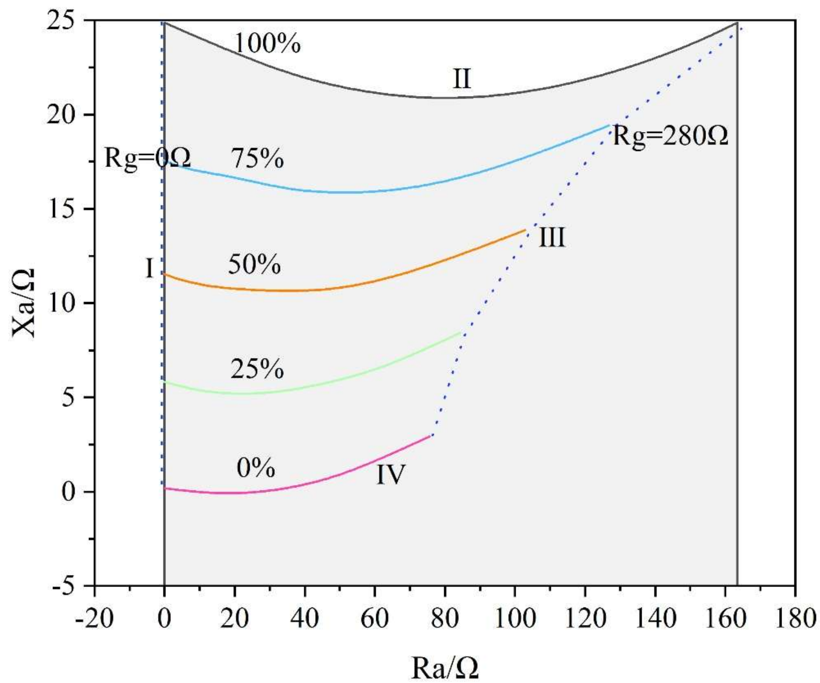

Fig. 10. The trajectory of the measured impedance changes at the different fault points

According to Fig. 10 it can be seen that no matter how the operating conditions change, the ideal operating region of the impedance relay in the protection Agent can be derived as shown in Fig. 11.

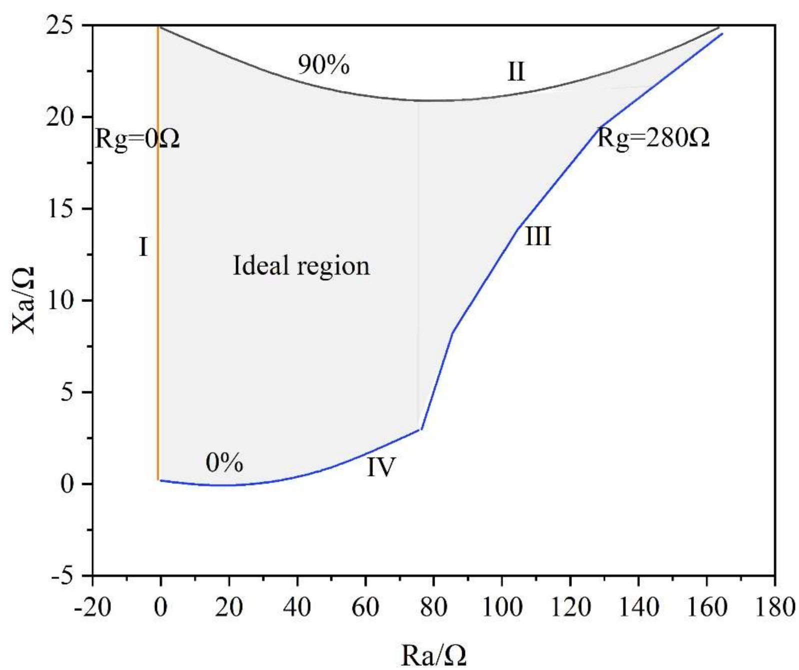

Fig. 11. Ideal action characteristic curve of the impedance relay

Let a and b be the action characteristic curves of offset characteristic impedance relay and multi-agent based adaptive impedance relay, respectively. According to this chapter, when a single-phase ground fault occurs in the system via the transition resistor, the offset characteristic impedance relay is easily affected by the gR, resulting in the range exceeding and mis-activation, while the multi-agent based adaptive protection has a better performance. Assuming that the total length of the line remains L=130km, the operation mode of b becomes 1.04, and the potential difference δ becomes 0°; the shift information of the switch is collected by WAMS in the executing Agent, and the data is transmitted to the protection Agent in the impedance relay. The data acquisition module in the coordinating Agent group, and then the topology analysis module utilizes the network maximum flow algorithm to carry out the connectivity of the network. The topology analysis module uses the network maximum flow algorithm to analyze the network connectivity and derive a topology analysis connectivity graph containing nodes and branches; the data obtained from the topology analysis is processed by the rectification calculation Agent group to derive a comprehensive zero sequence measurement impedance Z_{0M}, Z_{0N}. When the operation mode of the system is changed, the impedance relays in the protection Agents can update the data of the local side and the opposite side in a timely manner, and based on the change curve of the multiagent adaptive action characteristics, as shown in Fig. 12. The change curve of multi-agent based adaptive action characteristics is shown in Fig. 12.

When the decision-making Agent group confirms the tripping command, the action curve of the impedance relay in the protection Agent changes from a to b, which improves the reliability of protection. Through simulation analysis we can see that when a non-metallic short circuit occurs at the short circuit point, the multi-agent based impedance relay can adjust the protection range in real time and dynamically, so as to effectively counteract the transition resistance.

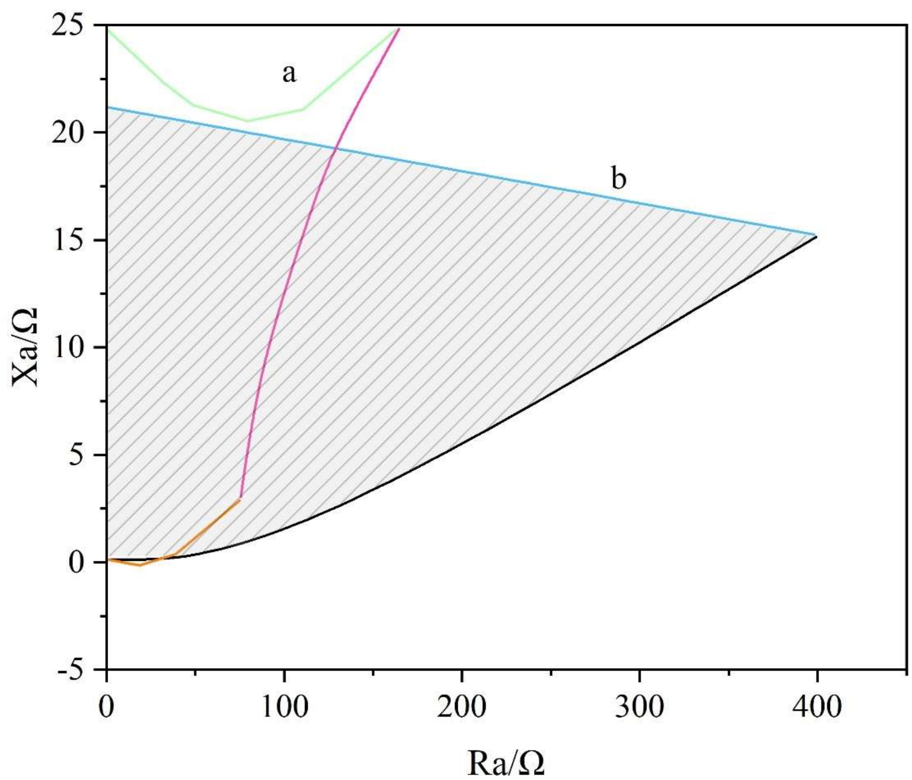

Fig. 12. Based on the multi-agent adaptive action characteristic changes

5. Conclusion

In this paper, we firstly design an AC/DC hybrid distribution network trend calculation and network loss analysis method based on the alternating iteration method, according to the established trend calculation model of the main equipment, the alternating iteration solution method is used for the trend analysis calculation and network loss calculation, and the feasibility of the proposed method is verified by two examples of AC/DC hybrid distribution networks. Finally, the MAS-based adaptive current interruption protection is combined with examples for simulation calculation, and the adaptive protection is combined with the hierarchical module-based multi-agent protection system, and the experimental results show that the multi-agent-based impedance relay can adjust the protection range in real time and dynamically, so as to effectively counteract the transition resistance.

Funding

This work was supported by the Supporting Special Topic 9 of Guangdong's "15th Five Year Plan" New Power System Planning: Research on Guangdong Power Grid's "15th Five Year Plan" Secondary System Planning (Project Number: 031000QQ00240021).

References

[1] Mirsaeidi, S., Dong, X., & Said, D. M. (2018). Towards hybrid AC/DC microgrids: Critical analysis and classification of protection strategies. Renewable and Sustainable Energy Reviews, 90, 97-103.

[2] Liu, X., Liu, Y., Liu, J., Xiang, Y., & Yuan, X. (2019). Optimal planning of AC-DC hybrid transmission and distributed energy resource system: Review and prospects. CSEE Journal of Power and Energy Systems, 5(3), 409-422.

[3] Wang, T., Li, C., Mi, D., Wang, Z., & Xiang, Y. (2020). Coordinated modulation strategy considering multi-HVDC emergency for enhancing transient stability of hybrid AC/DC power systems. CSEE Journal of Power and Energy Systems, 6(4), 806-815.

[4] Bui, D. M., Chen, S. L., Wu, C. H., Lien, K. Y., Huang, C. H., & Jen, K. K. (2014, December). Review on protection coordination strategies and development of an effective protection coordination system for DC microgrid. In 2014 IEEE PES Asia-Pacific Power and Energy Engineering Conference (APPEEC) (pp. 1-10). Ieee.

[5] Azeem, O., Ali, M., Abbas, G., Uzair, M., Qahmash, A., Algarni, A., & Hussain, M. R. (2021). A comprehensive review on integration challenges, optimization techniques and control strategies of hybrid AC/DC Microgrid. Applied Sciences, 11(14), 6242.

[6] Wang, X., & Kong, M. (2024). Transient characteristics and protection coordination strategy of hybrid AC/DC system based on modular multilevel converters under AC/DC transmission lines touching fault. Energy Reports, 11, 4213-4221.

[7] Mehdi, A., Hassan, S. J. U., Haider, Z., Arefaynie, A. D., Song, J. S., & Kim, C. H. (2024). A systematic review of fault characteristics and protection schemes in hybrid AC/DC networks: Challenges and future directions. Energy Reports, 12, 120-142.

[8] Mirsaeidi, S., Dong, X., Shi, S., & Tzelepis, D. (2017). Challenges, advances and future directions in protection of hybrid AC/DC microgrids. IET Renewable Power Generation, 11(12), 1495-1502.

[9] Gupta, A., Doolla, S., & Chatterjee, K. (2017). Hybrid AC–DC microgrid: Systematic evaluation of control strategies. IEEE Transactions on Smart Grid, 9(4), 3830-3843.

[10] Khan, M. Y. A., Liu, H., Zhang, Y., & Wang, J. (2024). Hybrid AC/DC Microgrid: Systematic Evaluation of Interlinking Converters, Control Strategies, and Protection Schemes: A Review. IEEE Access.

[11] Zhang, L., Wang, C., Liang, J., Wu, M., Zhang, B., & Tang, W. (2022). A coordinated restoration method of hybrid AC/DC distribution network for resilience enhancement. IEEE Transactions on Smart Grid, 14(1), 112-125.

[12] Liang, B., Kang, L., He, J., Zheng, F., Xia, Y., Zhang, Z., ... & Zhao, Y. (2019). Coordination control of hybrid

AC/DC microgrid. The Journal of Engineering, 2019(16), 3264-3269.

[13] Bharatee, A., Ray, P. K., Subudhi, B., & Ghosh, A. (2022). Power management strategies in a hybrid energy storage system integrated AC/DC microgrid: A review. Energies, 15(19), 7176.

[14] Agrawal, A., & Gupta, R. (2019). Distributed coordination control of hybrid energy resources for power sharing in coupled hybrid DC/AC microgrid using paralleled IFCs/ILCs. IET Smart Grid, 2(1), 89-105.

[15] Sun, P., Teng, Y., Leng, O., & Chen, Z. (2020). Stability control method for hybrid AC-DC transmission systems considering cross-region multi-energy coordination. CSEE Journal of Power and Energy Systems, 7(4), 753-760.

[16] Sarangi, S., Sahu, B. K., & Rout, P. K. (2020). Distributed generation hybrid AC/DC microgrid protection: A critical review on issues, strategies, and future directions. International Journal of Energy Research, 44(5), 3347-3364.

[17] Shu, Y., Chen, G., Yu, Z., Zhang, J., Wang, C., & Zheng, C. (2017). Characteristic analysis of UHVAC/DC hybrid power grids and construction of power system protection. CSEE Journal of Power and Energy Systems, 3(4), 325-333.

[18] Abdelwanis, M. I., & Elmezain, M. I. (2024). A comprehensive review of hybrid AC/DC networks: insights into system planning, energy management, control, and protection. Neural Computing and Applications, 36(29), 17961-17977.

[19] Dahane, A. S., & Sharma, R. B. (2024). Hybrid AC-DC microgrid coordinated control strategies: A systematic review and future prospect. Renewable Energy Focus, 100553.

[20] Wang, G., Wang, X., Wang, F., & Han, Z. (2020). Research on hierarchical control strategy of AC/DC hybrid microgrid based on power coordination control. Applied Sciences, 10(21), 7603.

[21] Prommetta, J., Schindler, J., Jaeger, J., Keil, T., Butterer, C., & Ebner, G. (2020). Protection coordination of ac/dc intersystem faults in hybrid transmission grids. IEEE Transactions on Power Delivery, 35(6), 2896-2904.

[22] Qian, Z., Yuan, Y., Li, J., Dong, H., Qin, T., Huang, X., ... & Wang, J. (2024). A Two-Stage Protection Scheme Based on Control and Protection Coordination For AC/DC Hybrid Distribution Network. IEEE Access.

[23] Chen, Z., Yan, J., & Lu, C. (2021). Coordinated control between prevention and correction of AC/DC hybrid power system based on steady-state security region. IEEE Access, 9, 47842-47855.

[24] Jiadong Cui,Jiahui Wang,Tengxiao Li,Ying Zhao,Jianwei Pan & Yongzhu Hua. (2024). Application of simplifying jacobian matrix and introducing iterative threshold to improve newton-raphson method in three-phase power flow calculation. Journal of Physics: Conference Series(1),012022-012022.

[25] Xue Yang,Enda Howley & Michael Schukat. (2024). Agent-based dynamic thresholding for adaptive anomaly detection using reinforcement learning. Neural Computing and Applications(prepublish),1-17.